American Mineralogist, Volume 78, pages 75–84, 1993

High-resolution transmission electron microscopy of polysomatism and stacking defects in antigorite

MAX T. OTTEN
Philips Electron Optics, Applications Laboratory, Building AAE, 5600 MD Eindhoven, The Netherlands

ABSTRACT

High-resolution TEM imaging of antigorite requires extreme care to minimize beam damage by using low-dose procedures for the setup and recording of images. Interpretation of fine image detail is possible only if the crystal is well aligned along its [010] zone axis, has not suffered much beam damage, and is thinner than about 15 nm. The high resolution achieved demonstrates that the conspicuous (100) fringe, observed in experimental but not in simulated images, corresponds to the antigorite half-wave reversal containing the six-membered rings of tetrahedra and not the one containing the eight-membered rings, as proposed previously.

Four types of microstructures occur in the antigorite studied: polysomatic variations in wavelength, produced by the addition or removal of lizardite modules; dislocations, where two antigorite waves merge into a single one, possibly with lizardite inserted where the wavelength becomes very long; **a**-glide twins, whose formation mechanism is probably due to attachment of a Mg cation to the wrong basal anion triad of an octahedron during nucleation of a new Mg octahedral sheet; and (100) offsets, where the wave reversals are shifted along $+\mathbf{a}$ or $-\mathbf{a}$ in steps of usually one, but occasionally more, lizardite modules, implying the occurrence of a single talc-like unit ($+\mathbf{a}$ shift) or a brucite-like unit ($-\mathbf{a}$ shift).

INTRODUCTION

The serpentine mineral antigorite has an unusual structure that allows considerable variation of the *a* lattice parameter, effectively making the model antigorite described by Kunze (1956, 1958, 1961) one of many possible antigorite structures. Additional forms are possible by variable stacking of the antigorite layers in the **c** direction. Several variations in structure were demonstrated (Spinnler, 1985; Livi and Veblen, 1987; Mellini et al., 1987), but the proposed structural mechanisms could not be demonstrated directly, because of the limited resolution of the transmission electron microscopes used. In this study, an antigorite specimen studied by Spinnler (1985) was reinvestigated to resolve the structural mechanisms directly.

PREVIOUS WORK

Kunze (1956, 1958, 1961) concluded from (*h*0*l*) data that the antigorite structure (Fig. 1) consists of a double half-wave that is made up of a sheet of Mg octahedra (the O sheet), with attached sheets of Si tetrahedra (the T sheets). The latter are always found on the inside of the half-waves. Reversals of direction of the apical O atoms in the T sheets occur every half wavelength. Two types of reversal boundaries alternate. The six-membered reversal (Spinnler, 1985) consists of a six-membered ring with three tetrahedra having apical O atoms pointing along $+\mathbf{c}$ and, on the opposite side of the reversal, the other three tetrahedra have their apical O atoms pointing along $-\mathbf{c}$. The eight-membered reversal has alternating four- and eight-membered rings of tetrahedra.

The variability of the *a* lattice parameter of antigorite may be described by considering the mineral as a polysomatic series, consisting of three modules (Fig. 2): lizardite modules, eight-membered modules, and six-membered modules (Spinnler, 1985). A unit cell contains a number of lizardite modules (each corresponding to one half of a lizardite unit cell), one eight-membered module (around the eight-membered reversal) and one six-membered module (around the six-membered reversal). The polysomatic series is constructed by varying the number of lizardite modules. Different polysomes may also be constructed by changing the distribution of the lizardite modules between the two half-waves, although strong asymmetries are unlikely to occur.

The following summarizes the microstructures found in antigorite by Spinnler (1985). HRTEM images of antigorite commonly display wavy (001) fringes that reflect the wave structure of the antigorite layers. In many images these fringes are discontinuous at the structural reversals. In addition to the wavy (001) fringes, the HRTEM images showed pronounced (100) fringes. The repeat of these (100) fringes is equivalent to the full wavelength (i.e., the whole unit cell), implying that only one type of reversal shows up in the image, whereas the other reversal remains indistinct. The latter reversal was also the site where beam damage is more severe than elsewhere in the structure, giving dark (100) fringes alternating with stripes of beam damage. Because of insufficient detail in the

0003–004X/93/0102–0075$02.00

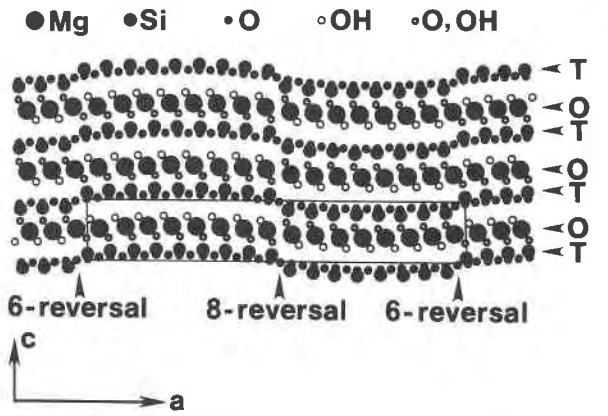

Fig. 1. The structure of antigorite (modified from Spinnler, 1985), showing the alternating half-waves, separated by the six-membered and eight-membered reversals. The unit cell is outlined.

HRTEM images, it could not be determined which of the two types of reversal produced the fringes and which one damaged so easily, but it was argued that the (100) fringe most likely occurred at the eight-membered reversal and the beam damage at the six-membered reversal. Some (100) fringes were found to terminate, producing a dislocation, where two antigorite waves merge into a single one.

The effects of the polysomatism were visible in the HRTEM images as wavelength changes. In some crystals the variations were quite noticeable, with alternating regions on the order of 30 nm wide, where the antigorite wavelength varies by more than a factor of two (e.g., Spinnler, 1985, his Fig. I-31). Within the accuracy of measurement, the unit of change between different wavelengths was found to be the width of a lizardite module (0.27 nm), consistent with the polysomatic model for the antigorite structure.

Two types of structural defects for the **c** direction were found: (001) twins and (100) fringe offsets. The twins, which are common in many of the antigorite crystals, cause a reversal of the stacking angle (β) in the antigorite. In addition, they display a shift of the dark (100) fringe

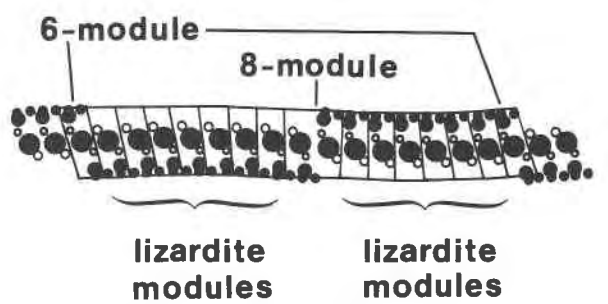

Fig. 2. Antigorite as a polysomatic series, showing the three types of modules: lizardite modules, the six-membered module, and the eight-membered module (after Spinnler, 1985). Legend for the atoms as in Fig. 1.

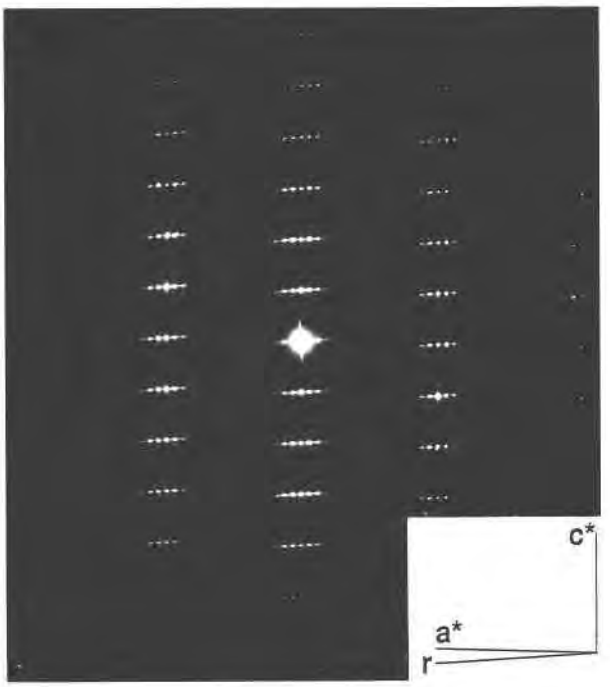

Fig. 3. A typical [010] diffraction pattern of the antigorite studied, displaying offsets between rows of satellites whose direction **r** deviates from **a***. The average *a* parameter apparent in the pattern is 4.6 nm (14 lizardite modules).

by **a**/2 across the twin boundary (an **a**-glide operation, hence the name **a**-glide twins). With this type of twin, the sense of curvature of the antigorite half-waves remains the same across the twin boundary, producing a close fit. Where many twins occur repeatedly, the antigorite takes on a checkerboardlike pattern (Spinnler, 1985, his Fig. I-24).

The (100) fringes in many crystals showed deviations from the proper **c** direction. In some cases the fringes were found to have offsets, which were presumed to be a single lizardite module wide. In other cases no offsets were visible, but the (100) fringes changed direction without any apparent cause, producing wobbles.

Together with the twins, the offsets and wobbles produce a deviation between the effective, overall **c** direction of the crystal and the **c** axis of the individual unit cells. This deviation is noticeable in diffraction patterns of the antigorite. These patterns display linear groups of closely spaced diffractions (Fig. 3). Each group reflects the lizardite sublattice, whereas the spacing of the diffractions within the groups reflects the large *a* dimension of the antigorite. For a perfect antigorite crystal, the groups of diffractions are aligned. For crystals that have twins or offsets, the groups of diffractions no longer align and can be rotated by up to 15° (Fig. 3).

Experimental technique

The antigorite specimen studied (referred to as Antig-MTO by Spinnler, 1985) was collected in the western

Italian Alps near Sestriere from an ophiolitic serpentinite, which underwent polyphase metamorphism, initially in the low-grade blueschist facies, followed by low-grade greenschist facies. It is not known whether the antigorite formed during the blueschist or the greenschist phase. The specimen consists entirely of antigorite. In hand specimen, it appears as a single crystal, having a bladed habit with prominent striations parallel to **b**. TEM analysis showed, however, that the specimen consists of many smaller grains, with the largest being about 1 μm thick (**c** direction) and 20 μm long (**a** direction). Many crystals show a preferred orientation, with **b** to within 15° of the perpendicular of the foil. The TEM specimen was prepared by ion milling a sample selected from a petrographic thin section. It was C-coated to prevent charging.

HRTEM images were made on a Philips CM30-Twin, operated at 300 kV with a point resolution of 0.23 nm. The coma-free alignment method (Zemlin, 1979) was used to align the objective lens with an accuracy of about 0.1 mrad. The effects of beam tilt, which can have pronounced effects on the HRTEM images (Smith et al., 1983; Self et al., 1985), were therefore avoided.

Antigorite, like the other serpentine minerals, damages rapidly in the electron beam (Yada, 1979; Veblen, 1980; Spinnler, 1985). Extensive beam damage occurs after only a few seconds of exposure to the high-intensity beam needed for high-resolution imaging. To minimize the damage, the low-dose mode of the CM30 was essential. With this mode, high-intensity illumination was used only during the actual photographic exposure, whereas focusing was done at much lower intensity using a Gatan 622 TV camera with image intensifier. A further reduction in beam damage was achieved by recording the images at a magnification of about 250 000×, which decreases the electron dose needed for photography by a factor of four in comparison with a more normal HRTEM magnification of 500 000×. In many images the antigorite crystals proved to be slightly tilted off the [010] zone axis because of the difficulty of aligning the small and often bent crystals while keeping the electron dose on the specimen to a minimum. Nevertheless, these images in many cases still yield valuable information.

HRTEM IMAGE SIMULATIONS

Image simulations were made on the basis of the half-wave model of Kunze (1956, 1958, 1961), with atom positions given by Spinnler (1985, his Appendix B). Mg and octahedral anion positions in the right-hand half-wave were corrected for the erroneous shift by $\mathbf{b}/\bar{2}$ in Spinnler (1985). This error involves a shift parallel to the HRTEM viewing direction [010] and therefore does not affect earlier results. The real-space method (Van Dyck and Coene, 1984; Coene and Van Dyck, 1984a, 1984b) was used for the image simulations. Microscope parameters used were accelerating voltage of 300 kV, C_s = 2.0 mm, defocus spread = 7 nm, beam divergence = 0.5 mrad, objective aperture = 7.1 nm^{-1}.

The simulations were performed for a range of specimen thicknesses. It was found that above approximately 15-nm thickness the images become very complex and poor in contrast. Together with additional complications introduced by crystal tilt and beam damage, the thickness effect makes it impossible to interpret fine detail in images from areas thicker than 15 nm.

Distinctive (100) fringes are usually absent in the simulated images. The contrast of such fringes, where present, is always considerably less pronounced than that observed in the experimental images. This discrepancy between experimental and simulated images may be related to the incoherent imaging contribution to such long-period features as the (100) fringes, which is not accounted for by coherent imaging theory.

For a range of focus settings the simulated images for thin areas display wavy lines of dots, alternatingly white and black (Fig. 4). For many of the simulated images, the lines of black dots roughly reflect the Mg and Si atom positions. The white dots are usually located near the empty tunnels between the Mg octahedra and the Si tetrahedra. A line of narrow tunnels occurs between the top of the Si tetrahedral sheet (top and bottom here refer to the left-hand half of the unit cell, cf. Fig. 1) and the bottom of the Mg octahedral sheet, i.e., the common junction of the tetrahedral and octahedral sheets. The contrast of this tunnel is generally lower than that of the wider tunnels, which occur in the interlayer region.

The white dots in the images form dumbbells across the Si tetrahedral sheet whose long axis is inclined to the **c** axis (Figs. 4, 5). The angle of inclination lies in the complement of the β angle, i.e., between $+\mathbf{c}$ and $-\mathbf{a}$ (in lizardite this is the $[\bar{1}01]$ direction, but in antigorite with its long and variable **a** axis such a notation becomes impossible). The dumbbells impart a pronounced directionality to the image, which allows a definitive determination of the crystallographic axes in the experimental image. Measuring the β angle is inconclusive in many instances because of its small deviation from 90°.

Improper crystal orientation away from the [010] zone produces a loss in resolution. If the crystal is tilted toward the **a** axis, the distinction between the individual white and black dots is lost, whereas the white dots of the wider tunnels remain visible up to higher tilt angles. The overall contrast in the two half-waves also becomes asymmetric. Such images are prominent in examples given by Yada (1979). If the tilt is toward the **c** axis, then the distinctive alternation of white dots and black dots is lost and is replaced by predominantly (002) and (h00) fringes (where h is equal to the number of lizardite modules plus three for the reversals). Crystal tilts can also result in a replacement of the regular waves of the layers by straight segments alternating with more abrupt waves.

IMAGE MATCHING

A number of experimental images, such as Figure 5, clearly show the wavy layers of continuous black dots and

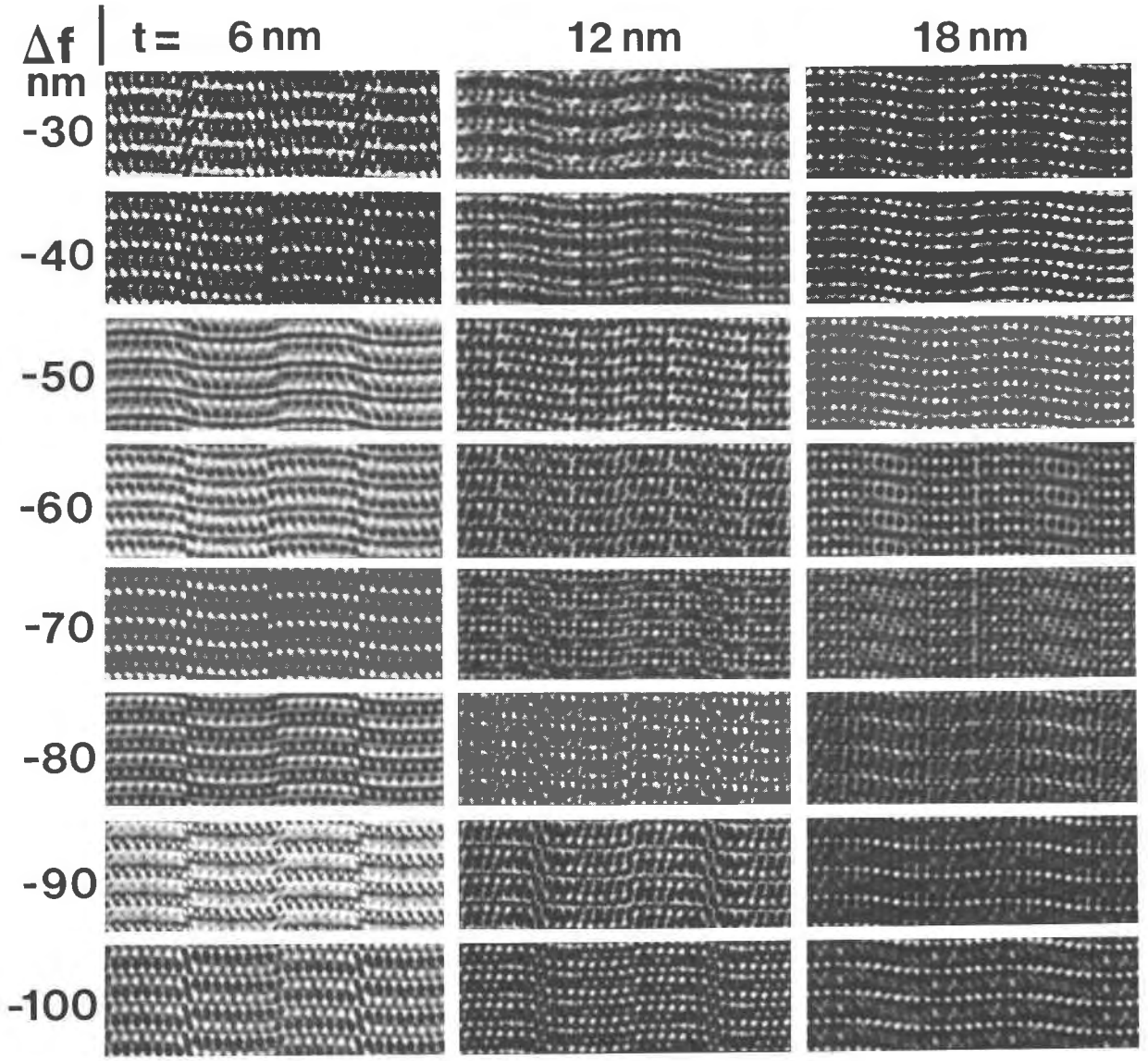

Fig. 4. Through-focus series of simulated images for specimen thicknesses of 6, 12, and 18 nm. Many of the images at 6 nm thick show dumbbells of white dots inclined to the left. The images at 12 and 18 nm are already complicated, making it nearly impossible to match simulated and experimental images for thicknesses of more than 15 nm.

of discontinuous white dots as well as the dumbbells, although reversals do not align everywhere because of the variation of the a repeat and the occurrence of (100) offsets in the experimental image. The sense of inclination of the dumbbells, the β angle, and the waves match closely with the simulated images. To obtain this match, it was necessary to deviate from the location of the six-membered and eight-membered reversals proposed by Spinnler (1985). Image comparison clearly shows that the six-membered reversal coincides with the (100) fringe, whereas the eight-membered reversal occurs in the region more easily damaged by the beam. The high resolution obtained in the present study provides sufficient detail to allow a direct determination of the location of the reversals, in contrast to the earlier study (Spinnler, 1985).

Noise and beam damage preclude the determination of finer detail, such as the structure of the reversals. Yada (1979) used image processing methods to yield an average structure with much more detail than the raw experimental image. However, image processing is not recommended in HRTEM imaging, since the results of such methods are based on unverifiable assumptions. The use of image processing on the antigorite, with its highly variable wavelength and (100) offsets, would produce a near-perfect image without physical basis, since the image is an average of a series of different structures.

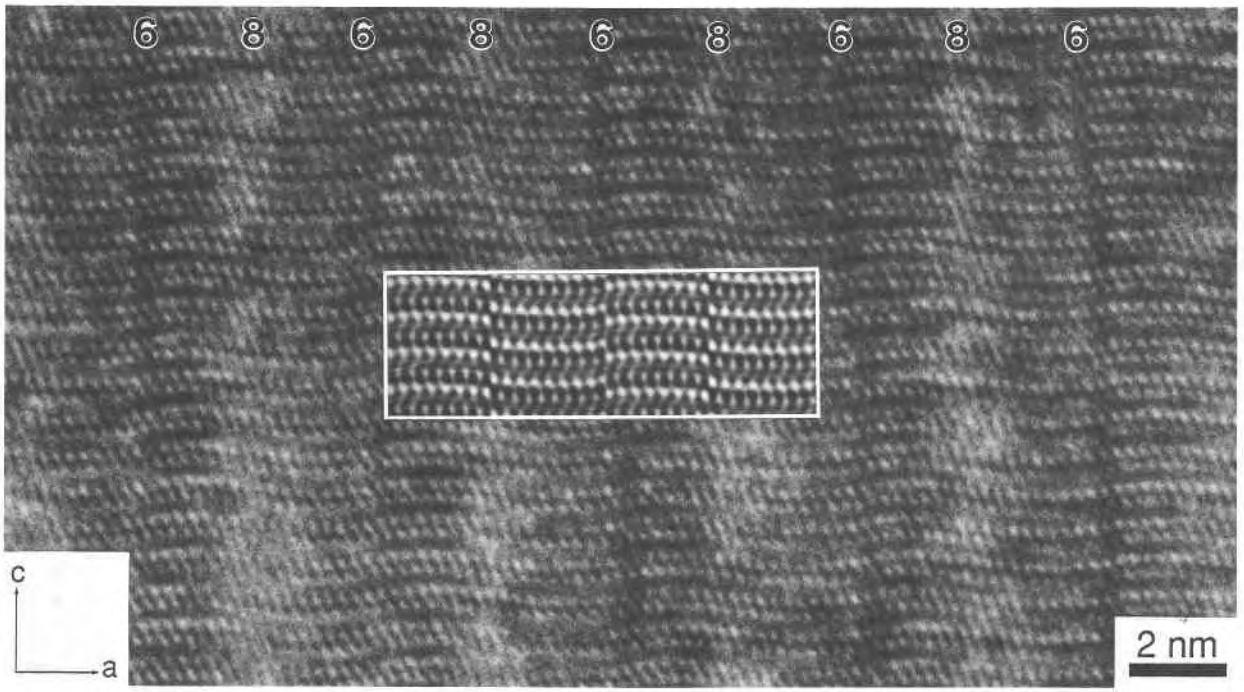

Fig. 5. Match between an experimental and a simulated image. Both experimental and simulated images show the same wavy layers of black dots (one layer more continuous than the other) and white dots. The inclination direction of the pairs of white dots, looking like dumbbells, the β angle, and the curvature of the waves are matched only if the six-membered reversal occurs at the position of the (100) fringe.

Experimental observations

Polysomatism

Changes in wavelength are so pervasive in the antigorite studied that areas where adjacent waves have the same polysomatic structure and some continuity in the **c** direction are uncommon. Changes in wavelengths are obvious at lower magnifications from the spacings of (100) fringes. In some crystals the distribution of the wavelengths occurs in waves, producing an accordionlike texture (Fig. 6; cf., also Spinnler, 1985, his Fig. I-31).

The pattern of white dots (Figs. 5, 7, 8) in higher-magnification images makes it possible to count lizardite modules in a single wave, i.e., the number of white dots from one (100) fringe to the next with three subtracted for the reversal modules (one for the six-membered module, two for the eight-membered module). Even in images where the white dots are indistinct, it usually is still possible to count lizardite modules from the (h00) fringes, which have the same spacing as the white dots.

The total span of polysomes observed varies from a minimum of 3 nm with eight lizardite modules to ones well over 10 nm wide with more than 40 lizardite modules. The most abundant polysomes are in the range of 13 to 25 lizardite modules. Even and odd numbers are equally common. Polysomes with fewer than ten or more than 30 lizardite modules are observed only near modulation dislocations (Fig. 7).

The origin of the variability in wavelength is not apparent. The corrugation of the antigorite structure may originate from the misfit between the octahedral and tetrahedral sheets (Bailey, 1984), with the wavelength determined by the degree of misfit. Changes in composition, such as substitution of Al for Si (enlarging the T sheet) or substitution of Fe^{3+} for Mg (decreasing the O sheet) could lead to smaller misfits and increased wavelengths. This hypothesis could not be tested by chemical analysis of regions with different wavelength, because chemical changes due to beam damage, measured from two consecutive 30-s X-ray spectra of the same area, yielded far greater differences in Mg and Fe (up to 20% decrease of both Mg and Fe relative to Si, which remains roughly constant) than different areas (less than 5%). Variations of Al content can be discounted, however, because the antigorite does not contain any Al.

Modulation dislocations

Occasionally antigorite waves are found to terminate at modulation dislocations (Figs. 7, 8). Many of these dislocations are associated with extreme cases of (100) offsets and wavelength variations. Some occur in pairs of opposite sign (Fig. 7), with a strongly distorted structure between them.

The internal structure of the modulation dislocations remains unclear, because they were found only in thicker specimen areas, where image contrast cannot be interpreted. The image of one dislocation in a thinner area

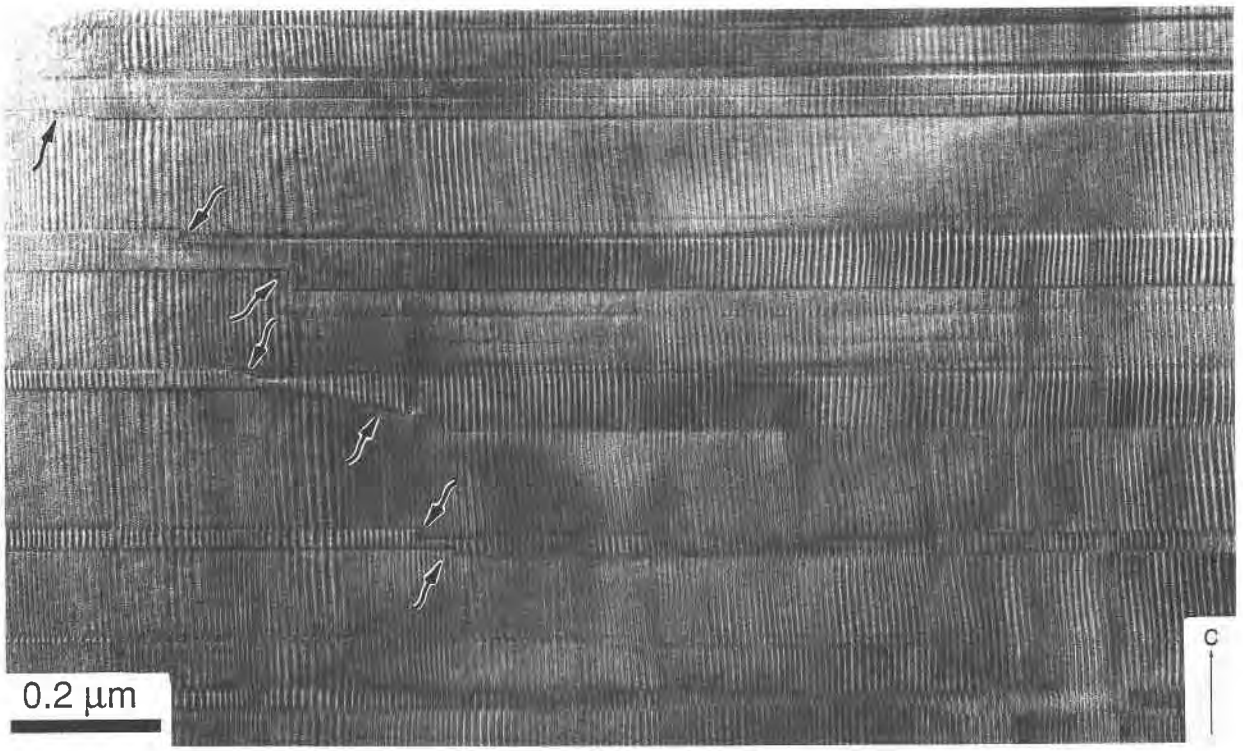

Fig. 6. Lower-magnification image of antigorite, showing pronounced wavelength changes (accordionlike effect) as well as abundant (001) twins, some of which show irregular terminations within the antigorite (arrows).

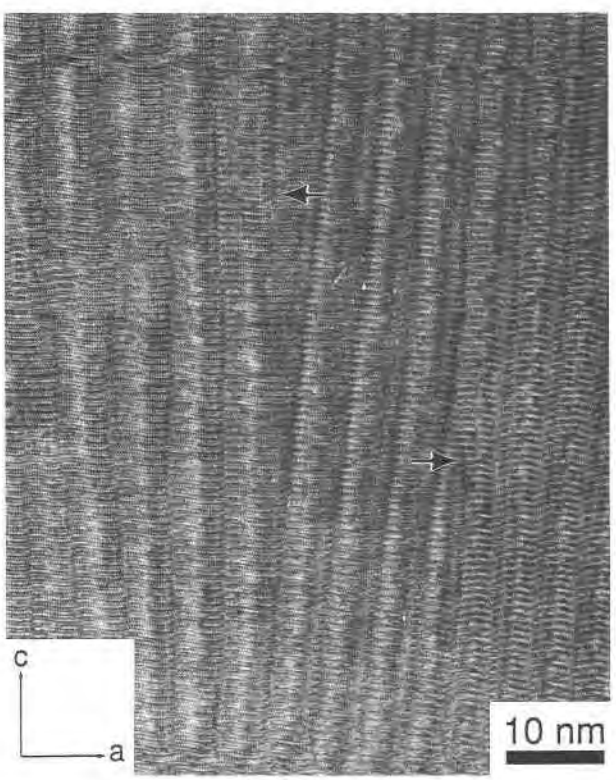

(Fig. 8) suggests that in some cases the extreme wavelength changes may be related to the insertion of a stack of flat lizardite layers that disappears where the modulations have fewer than about 30 lizardite modules. This interpretation is tentative because straight segments, instead of corrugated layers, are observed in the same image because of crystal tilt.

Twins

The twin operation in antigorite can be described by a (001) mirror in combination with a shift of **a**/2, i.e., an **a**-glide operation (Spinnler, 1985). This combination ensures that the antigorite half-waves remain in phase across the twin boundary and that the six-membered and eight-

←

Fig. 7. HRTEM image of antigorite showing two modulation dislocations (arrows) of opposite sign. Both cause rather extreme changes in wavelength (16 to 35 lizardite modules for the left-hand dislocation, 5 to 20 lizardite modules for the right-hand one). They are also associated with abundant (100) offsets. Whereas the (100) fringe left of the left-hand dislocation is almost straight, the fringe to the right has on average one offset per three layers. The internal structure of the dislocations cannot be determined because of specimen thickness.

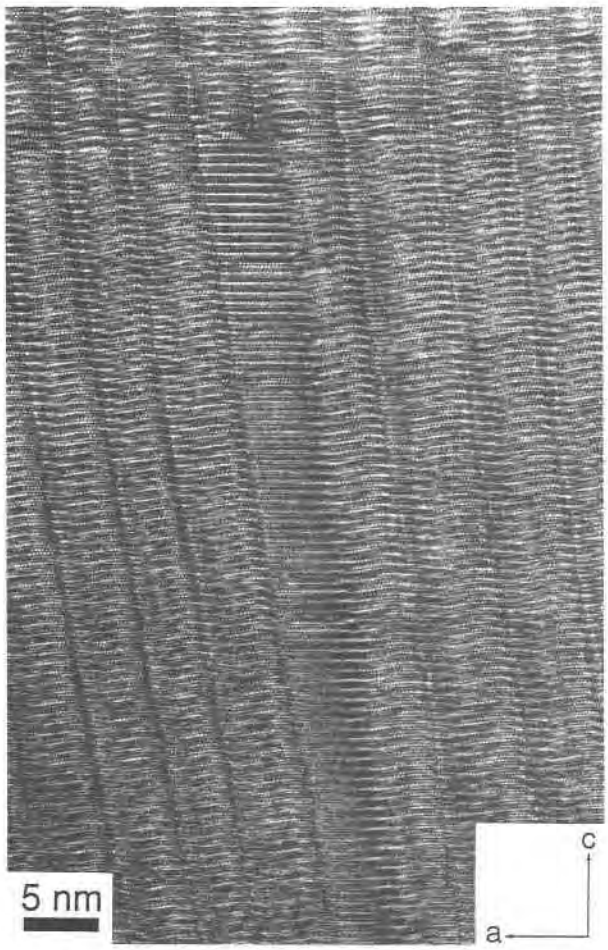

membered reversals switch position, as observed in the experimental images (Fig. 9).

The occurrence of twins is variable. Some crystals contain no twins, whereas adjacent grains are twinned frequently, with uninterrupted stacking sequences limited to 10–20 nm. Strongly disordered stacking is common, with an **a**-glide operating every few *c* periodicities. In extreme cases, twins occur every unit cell, resulting in a two-layer polytype, but this type of structure is not common.

Twins are detected easily at lower magnification, especially if the antigorite [010] direction is not perfectly parallel to the beam. In such low-magnification images, it is apparent that not all twin domains are continuous across the full length of the crystal and that some have terminations parallel to (100) (Figs. 6, 9).

Although difficult to resolve directly, a twin-boundary model may be constructed on the basis of the ideal antigorite structure. A tetrahedral sheet that is fully extended and with symmetrical six-membered rings is common to both twin components. The sheet of Mg octahedra has

←

Fig. 8. Straight lines of white dots below a modulation dislocation in a thinner area suggest that part of the change in wavelength is relieved by the insertion of flat lizardite layers. Caution is necessary, however, because the antigorite itself also shows apparently straight segments, instead of wavy layers, because of a crystal misalignment. A twin runs through the crystal where the modulation dislocation occurs. The overall stacking direction deviates between 5 and 10° from the unit-cell **c** axis, as shown by the small segments of straight (100) fringes (vertical in the figure; for example, to the right of the dislocation).

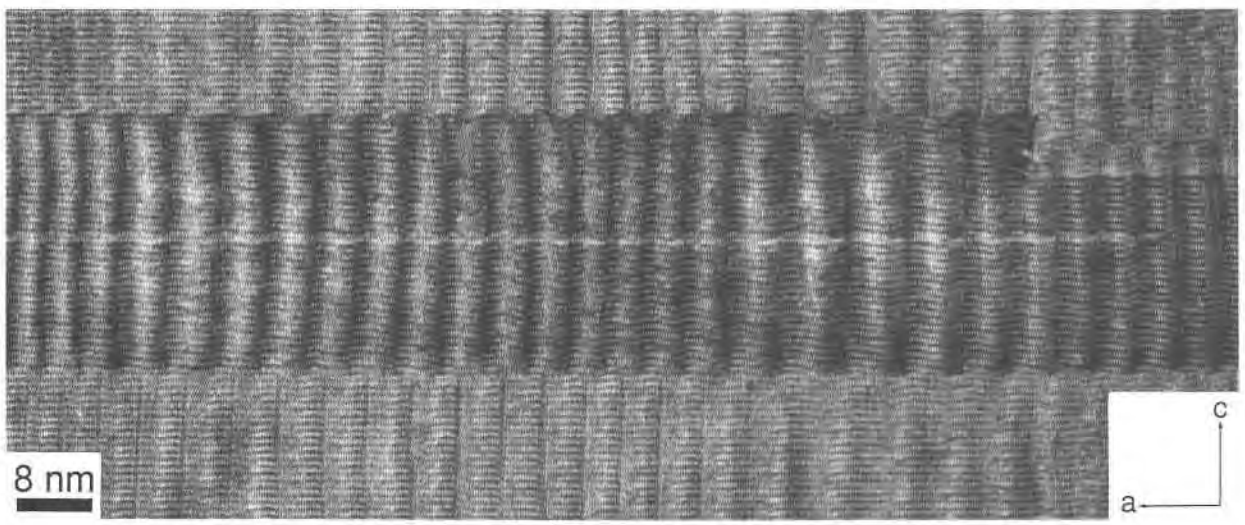

Fig. 9. HRTEM image of a large **a**-glide twin, showing the shift of the (100) fringes by **a**/2. The twin shows an abrupt decrease of thickness by nine antigorite layers. It contains a thinner twin that is only two layers thick. The antigorite in the center of the thicker part of the twin has a large number of (100) offsets, whereas closer to the twin boundaries the structure is more regular, as shown by straight (100) fringes.

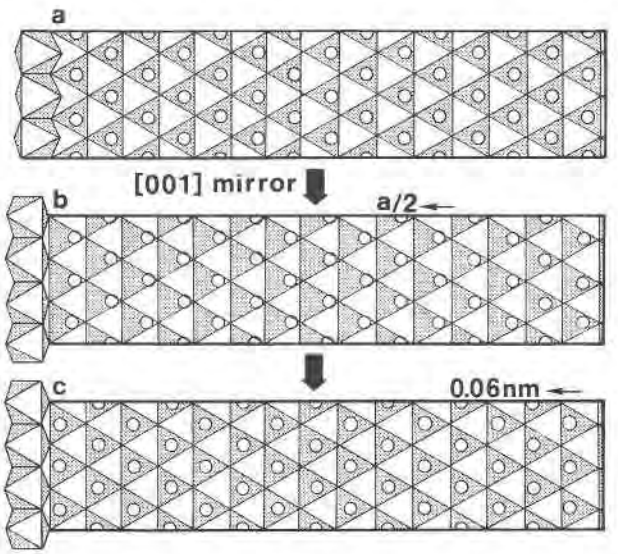

a pronounced directionality, with the lower anion triad of the octahedra pointing toward **−a** (Fig. 10). It is the Mg octahedral sheets therefore that distinguish the twin orientation.

The twin may be constructed by applying a (001) mirror to the structure at the Mg plane and shifting it by **a**/2 (Fig. 10b). The Mg ions will then be above the triads of anions that point toward the **+a** direction, as they should for the twin orientation. A shift of 0.06 nm (about 20%

←

Fig. 10. The Mg octahedral sheet seen from above, with most of the top O layer removed. In the ideal structure (**a**), Mg is roughly centered above triads (shaded) of anions that point in the **−a** direction. (The centering of the Mg is not perfect in projection because of the tilting of the octahedra in the antigorite waves.) A (001) mirror plus an **a**/2 shift produce the twin orientation (**b**), with Mg now above triads pointing in the opposite direction. A small additional shift of 0.06 nm is needed (**c**) to center the Mg layer correctly above the anion triads.

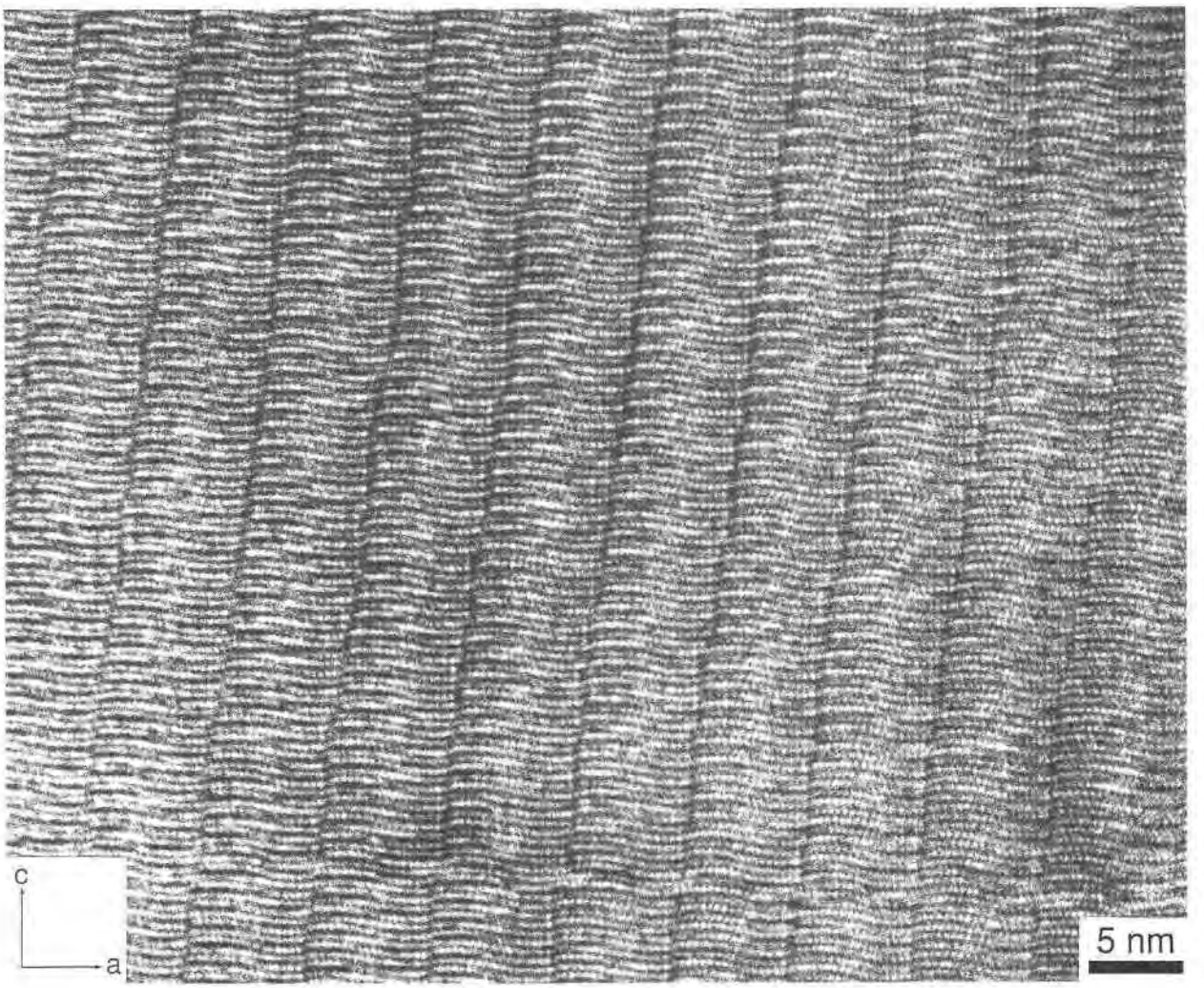

of the width of a lizardite module) is required to center the Mg ions on the anion triads to maintain closest packing (Fig. 10c). The shift is canceled at the next twin boundary by the reverse twin operation. The shift was not detected in the images, possibly because it is too small.

The origin of the **a**-glide twin is based on the distinction between the two tilt orientations of the Mg octahedra, which is related to the direction in which the basal anion triad of the Mg octahedra points. If, during the growth of antigorite, the first Mg cation of a new octahedral sheet attaches to the apical O atoms of a Si tetrahedral sheet in the wrong triad, other Mg cations attaching to adjacent triads would follow the pattern, thereby creating a twin. Starting growth of a new octahedral sheet from multiple nuclei leads to the two twin orientations growing toward each other in a single sheet, producing (100) twin terminations, as observed in the experimental images (Fig. 6).

Fringe offsets

Lateral shifts between adjacent layers and variations in wavelength are common in the antigorite. Both are accommodated by lateral shifts of the reversals in the structure. Where a single reversal shifts sideways, one unit cell increases its wavelength at the expense of the adjacent unit cell. Where all reversals in a layer are shifted sideways together, the whole layer is shifted along **+a** or **−a**, but no changes in wavelength are incurred. In that case, (100) fringes are seen to wobble. The wobbles described by Spinnler (1985) are most likely not a separate phenomenon but simply abundant (100) fringe offsets, where the fringe itself is too indistinct to allow direct observation of the wobble mechanism.

The lateral shifts are observed as offsets of the (100) fringe that marks the position of the six-membered reversal (Fig. 11). The eight-membered reversal must be shifted too but is not resolved in the HRTEM images. The (100) fringe offsets produce an effective **c** direction that differs from the **c** axis of the individual unit cells, thereby causing the rotation of the groups of diffractions in the diffraction pattern (Fig. 3). High offset densities produce larger angular deviations from the unit-cell **c** axis.

Viewing images with (100) offsets at a small angle to the page parallel to the unit-cell **c** axis shows that only the position of the six-membered module is affected by the offsets. The (*h*00) fringes, located between the (100) fringes, are straight, implying that the width of the offsets

←

Fig. 11. HRTEM image of antigorite showing abundant offsets where the six-membered reversals are displaced by one lizardite module relative to the same reversal in the under- or overlying unit cell. The offsets are best visible when looking along **c** at a low angle to the page. If the stacking were perfect, the broad (100) fringes of the six-membered reversals would be parallel to the thinner (*h*00) fringes adjacent to them. Instead the six-membered reversals go off at an angle of about 5° to the normal stacking angle (parallel to the vertical direction in the micrograph).

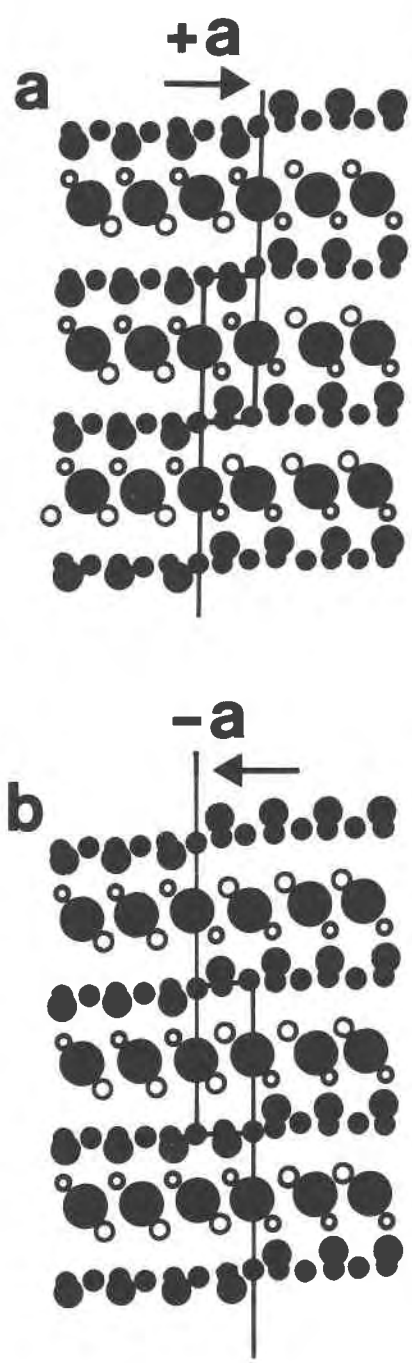

Fig. 12. Projection of the part of the antigorite structure around the six-membered reversals for two directions of offsets. (**a**) Offsets in the **+a** direction lead to the occupation of both tetrahedral sites on opposite sides of the O sheet (a talc-like unit in the box between the reversals), whereas offsets parallel to **−a** (**b**) lead to the presence of a vacant tetrahedral site (a brucite-like unit). The vertical lines mark the reversals. Legend for the atoms as in Fig. 1.

is an integral number of lizardite modules. Offsets wider than one lizardite module were observed but are rare.

Offsets parallel to **+a** are expected to be energetically different from those parallel to **−a**. Thus the structure would tend to stagger in one direction. For a shift in the **+a** direction, an additional tetrahedral site is occupied (Fig. 12a), which corresponds to the presence of one T-O-T (talc-like) unit in the T-O structure of antigorite. A **−a** shift results in a vacant tetrahedral site and thus a brucite-like unit (O structure) is inserted. Wherever determined, the talc-like unit (**+a** direction) offset was predominant.

The origin of the (100) fringe wobbles and offsets is unclear. A chemical origin is unlikely, because the effect for one reversal (e.g., a talc-like unit with one additional Si tetrahedron) is canceled by the formation of a brucite-like unit at the other type of reversal. Crystallographic constraints probably limit offsets to a single lizardite module, because offsetting the reversals too far in adjacent layers would make it difficult for the waves to fit together.

Acknowledgments

I would like to thank Gerard E. Spinnler (Shell Development Company, Houston) for getting me involved with antigorite while at Arizona State University and for the many discussions since then. Wim M.J. Coene (Philips Research Laboratories, Eindhoven, The Netherlands) kindly assisted with the image simulations. A.L.M. van Hooff did the photography work.

References cited

Bailey, S.W. (1984) Crystal chemistry of the true micas. In Mineralogical Society of America Reviews in Mineralogy, 13, 13–60.

Coene, W., and Van Dyck, D. (1984a) The real space method for dynamical electron diffraction calculations in high resolution electron microscopy. II. Critical analysis of the dependency on the input parameters. Ultramicroscopy, 15, 41–50.

——— (1984b) The real space method for dynamical electron diffraction calculations in high resolution electron microscopy. III. A computational algorithm for the electron propagation with its practical applications. Ultramicroscopy, 15, 287–300.

Kunze, V.G. (1956) Die gewellte Struktur des Antigorits, I. Zeitschrift für Kristallographie, 108, 82–107.

——— (1958) Die gewellte Struktur des Antigorits, II. Zeitschrift für Kristallographie, 110, 282–320.

——— (1961) Antigorit. Fortschritte der Mineralogie, 39, 206–324.

Livi, K.J.T., and Veblen, D.R. (1987) "Eastonite" from Easton, Pennsylvania: A mixture of phlogopite and a new form of serpentine. American Mineralogist, 72, 113–125.

Mellini, M., Trommsdorff, V., and Compagnoni, R. (1987) Antigorite polysomatism: Behavior during progressive metamorphism. Contributions to Mineralogy and Petrology, 97, 147–155.

Self, P.G., Glaisher, R.W., and Spargo, A.E.C. (1985) Interpreting high-resolution transmission electron micrographs. Ultramicroscopy, 18, 49–62.

Smith, D.J., Saxton, W.O., O'Keefe, M.A., Wood, G.J., and Stobbs, W.M. (1983) The importance of beam alignment and crystal tilt in high resolution electron microscopy. Ultramicroscopy, 11, 263–281.

Spinnler, G.E. (1985) HRTEM study of antigorite, pyroxene-serpentine reactions and chlorite. Ph.D. thesis, Arizona State University, Tempe, Arizona.

Van Dyck, D., and Coene, W. (1984) The real space method for dynamical electron diffraction calculations in high resolution electron microscopy. I. Principles of the method. Ultramicroscopy, 15, 29–40.

Veblen, D.R. (1980) Anthophyllite asbestos: Microstructures, intergrown silicates, and mechanisms of fiber formation. American Mineralogist, 65, 1075–1086.

Yada, K. (1979) Microstructures of chrysotile and antigorite by high-resolution electron microscopy. Canadian Mineralogist, 17, 679–691.

Zemlin, F. (1979) A practical procedure for alignment of a high resolution electron microscope. Ultramicroscopy, 4, 241–245.

Manuscript received January 14, 1992
Manuscript accepted August 24, 1992